

Unveiling the role of high-order anharmonicity in thermal expansion: A first-principles perspective

Tianxu Zhang(张天旭), Kun Zhou(周琨), Yingjian Li(李英健), Chenhao Yi(易晨浩), Muhammad Faizan, Yuhao Fu(付钰豪), Xinjiang Wang(王新江), and Lijun Zhang(张立军)

Citation : Chin. Phys. B, 2025, 34 (**4**): 046301. DOI: 10.1088/1674-1056/adb94c
Journal homepage: http://cpb.iphy.ac.cn; http://iopscience.iop.org/cpb

What follows is a list of articles you may be interested in

First-principles study of electronic and magnetic properties of self-intercalated van der Waals magnet $Cr_3Ge_2Te_6$

Jia-wan Li(李家万), Shi-Bo Zhao(赵世博), Lin Zhuang(庄琳), and Yusheng Hou(侯玉升)
Chin. Phys. B, 2025, 34 (**3**): 036301. DOI: 10.1088/1674-1056/adab67

Stable structures and properties of Ru_2Al_5

Jing Luo(罗晶), Meiguang Zhang(张美光), Xiaofei Jia(贾晓菲), and Qun Wei(魏群)
Chin. Phys. B, 2025, 34 (**1**): 016301. DOI: 10.1088/1674-1056/ad92fe

Strain-tuned electronic and valley-related properties in Janus monolayers of SWSiX_2 (X = N, P, As)

Yunxi Qi(戚云西), Jun Zhao(赵俊), and Hui Zeng(曾晖)
Chin. Phys. B, 2024, 33 (**9**): 096302. DOI: 10.1088/1674-1056/ad6077

Optical spectrum of ferrovalley materials: A case study of Janus H-VSSe

Chao-Bo Luo(罗朝波), Wen-Chao Liu(刘文超), and Xiang-Yang Peng(彭向阳)
Chin. Phys. B, 2024, 33 (**1**): 016303. DOI: 10.1088/1674-1056/acf660

Determining Hubbard U of VO_2 by the quasi-harmonic approximation

Longjuan Kong(孔龙娟), Yuhang Lu(陆雨航), Xinying Zhuang(庄新莹), Zhiyong Zhou(周志勇), and Zhenpeng Hu(胡振芃)
Chin. Phys. B, 2024, 33 (**1**): 016302. DOI: 10.1088/1674-1056/acfd18

RAPID COMMUNICATION

Unveiling the role of high-order anharmonicity in thermal expansion: A first-principles perspective

Tianxu Zhang(张天旭)[1,†], Kun Zhou(周琨)[1,†], Yingjian Li(李英健)[1], Chenhao Yi(易晨浩)[2], Muhammad Faizan[1], Yuhao Fu(付钰豪)[3,4], Xinjiang Wang(王新江)[1,‡], and Lijun Zhang(张立军)[1,4]

[1] *State Key Laboratory of Integrated Optoelectronics Key Laboratory of Automobile Materials of the Ministry of Education, and College of Materials Science and Engineering, Jilin University, Changchun* 130012, *China*
[2] *Jiangxi Guanyi Grinding Co., Ltd., Fengxin* 330700, *China*
[3] *State Key Laboratory of Superhard Materials, College of Physics, Jilin University, Changchun* 130012, *China*
[4] *International Center of Computational Method and Software, Jilin University, Changchun* 130012, *China*

(Received 17 January 2025; revised manuscript received 22 February 2025; accepted manuscript online 24 February 2025)

Thermal expansion is crucial for various industrial processes and is increasingly the focus of research endeavors aimed at improving material performance. However, it is the continuous advancements in first-principles calculations that have enabled researchers to understand the microscopic origins of thermal expansion. In this study, we propose a coefficient of thermal expansion (CTE) calculation scheme based on self-consistent phonon theory, incorporating the fourth-order anharmonicity. We selected four structures (Si, $CaZrF_6$, $SrTiO_3$, NaBr) to investigate high-order anharmonicity's impact on their CTEs, based on bonding types. The results indicate that our method goes beyond the second-order quasi-harmonic approximation and the third-order perturbation theory, aligning closely with experimental data. Furthermore, we observed that an increase in the ionicity of the structures leads to a more pronounced influence of high-order anharmonicity on CTE, with this effect primarily manifesting in variations of the Grüneisen parameter. Our research provides a theoretical foundation for accurately predicting and regulating the thermal expansion behavior of materials.

Keywords: high-order anharmonicity, Grüneisen parameter, thermal expansion, first-principles calculations

PACS: 63.20.dk, 65.40.De

DOI: 10.1088/1674-1056/adb94c **CSTR:** 32038.14.CPB.adb94c

1. Introduction

The thermal expansion of solids plays a vital role in describing various physical properties, such as thermodynamic functions, volume-dependent phonon frequencies, and bulk modulus. This makes it a key area of research in condensed matter physics and materials science. Recent advances in first-principles calculations based on density functional theory have led to extensive studies of materials exhibiting negative and zero thermal expansion, which have important applications in precision engineering.[1–7] However, due to the complexity of lattice anharmonicity, accurately predicting the coefficient of thermal expansion (CTE) for complex materials remains challenging. Therefore, overcoming the limitations of current computational methods and gaining a deeper understanding of the physical mechanisms behind thermal expansion is crucial for refining research outcomes and designing new materials with tailored properties.

The quasi-harmonic approximation (QHA) is the most widely used method for studying thermal expansion, based on the assumption that the potential energy surface is nearly harmonic while neglecting all anharmonic effects except for the volume dependence of phonon frequencies.[8] Due to its relatively low computational cost and ability to provide thermal expansion coefficients for a wide range of temperature, QHA has been widely applied to explain experimental phenomena and predict novel materials.[9–11] However, QHA overlooks temperature induced changes in phonon frequencies, making it less reliable at temperatures near the melting point or in materials that exhibit strong anharmonicity, as demonstrated in the case of NaBr.[12] Furthermore, QHA cannot be applied to systems with unstable phonon modes under harmonic approximation, such as perovskites and certain thermoelectric materials.

Perturbation theory (PT), which assumes that the anharmonic terms of the potential energy surface are relatively small compared to the harmonic terms, accounts for the contribution of cubic terms and is widely used to explain phonon linewidths and calculate lattice thermal conductivity.[13–16] In PT, the Grüneisen parameter, a key parameter of CTE, is derived from harmonic and cubic force constants. The force constant can be obtained through methods such as the supercell finite displacement or temperature-dependent effective poten-

[†]These anthors contributed equally to this work.
[‡]Corresponding author. E-mail: xinjiang_wang@jlu.edu.cn
© 2025 Chinese Physical Society and IOP Publishing Ltd. All rights, including for text and data mining, AI training, and similar technologies, are reserved.

tial (TDEP) method.[17–19] By combining PT and TDEP, researchers have found that inorganic halide perovskites exhibit larger CTE than oxide counterparts, attributed the deviations between calculated and experimental results to the omission of higher-order terms.[20] Furthermore, recent studies have revealed that the fourth-order anharmonic interactions play a significant role in thermal expansion, as demonstrated in materials such as ScF_3, MgO, and NaCl. This highlights the need to optimize computational models to improve predictive accuracy.[21,22]

The self-consistent phonon (SCPH) theory, originally developed by Hooton and further refined through many-body theory, provides a nonperturbative approach capable of addressing the anharmonic renormalization of phonon frequencies.[23,24] Implementing SCPH requires the fourth-order force constants, which can be extracted from DFT calculations using the compressive sensing lattice dynamics (CSLD) method, as proposed by Zhou Fei.[25,26] Due to its ability to analyze strongly anharmonic systems, this method has been widely applied to calculate renormalized phonon frequencies and lattice thermal conductivity in materials such as perovskites and anti-perovskites.[27,28]

In this study, we propose a scheme based on SCPH theory that includes higher-order terms to calculate the CTE. First, we obtain the anharmonically renormalized phonon frequencies, or effective harmonic force constants, through the CSLD method and SCPH theory. Next, we redefine the lattice heat capacity and Grüneisen parameter by combining PT with the solution of the SCPH equation. Finally, we calculate the volumetric CTE of the material using Grüneisen's law.[29] Since bonding composition determines the properties of materials, we selected four structures from the perspective of bond types: covalent crystal Si, mixed-bonded $CaZrF_6$ and $SrTiO_3$, and ionic crystal NaBr. We conducted an in-depth analysis of the relationship between the impact of higher-order terms on thermal expansion and bond types.

2. Methodology

We first express the potential energy of the crystal as a Taylor series expansion with respect to the atomic displacements:

$$U - U_0 = U_2 + U_3 + U_4 + \cdots, \tag{1}$$

$$U_n = \frac{1}{n!}\sum\nolimits_{\{l,\kappa,\mu\}} \Phi_{\mu_1\ldots\mu_n}(l_1\kappa_1;\ldots;l_n\kappa_n) \times u_{\mu_1}(l_1\kappa_1)\cdots u_{\mu_n}(l_n\kappa_n). \tag{2}$$

Here, $u_\mu(l\kappa)$ is the displacement of atom κ in the l-th unit cell along the ($\mu = x, y, z$) direction and $\Phi_{\mu_1\ldots\mu_n}(l_1\kappa_1;\ldots;l_n\kappa_n)$ is the n-th-order derivative of the potential energy with respect to displacement, commonly referred to as the interatomic force constants (IFCs).

By utilizing harmonic and quartic IFCs, we can derive the following self-consistent phonon equation to solve for the renormalized phonon frequencies (self-consistent phonon frequencies) Ω_q^{scph}.

$$\Omega_{\boldsymbol{q}}^2 = w_{\boldsymbol{q}}^2 + 2\Omega_{\boldsymbol{q}} I_{\boldsymbol{q}}, \tag{3}$$

$$I_{\boldsymbol{q}} = \sum\nolimits_{q_1} \frac{\hbar(\boldsymbol{q};-\boldsymbol{q};q_1;-q_1)}{4\Omega_{\boldsymbol{q}}\Omega_{q1}} \frac{\left[2n_{\mathrm{B}}\left(\Omega_{q1}\right)+1\right]}{2}, \tag{4}$$

where $w_{\boldsymbol{q}}$ represents the phonon frequency under the harmonic approximation, q_1 is the inner-loop iteration grid for the SCPH equation, and $\hbar$ and n_{B} are respectively the reduced Planck constant and the Bose–Einstein distribution function. The explicit temperature dependence of the distribution function allows temperature-specific renormalized phonon frequencies to be derived, directly generating finite-temperature phonon dispersion spectra.

Using Ω_q^{scph}, we redefine the mode heat capacity as

$$C_{V,\boldsymbol{q}j}^{\mathrm{SCPH}}(T) = \hbar\Omega_{\boldsymbol{q}j}\frac{\partial n_{\mathrm{B}}(\Omega_{\boldsymbol{q}j})}{\partial T}, \tag{5}$$

where the index j labels the phonon modes for each crystal momentum vector $\boldsymbol{q}$ and T is the temperature. By combining PT and Ω_q^{scph}, we redefine the mode Grüneisen parameter as

$$\gamma_{\boldsymbol{q}j}^{\mathrm{SCPH}}(T) = -\frac{\partial \ln\Omega_{\boldsymbol{q}j}}{\partial \ln V} = -\frac{\left(\boldsymbol{e}_{\boldsymbol{q}j}^{\prime *}\right)^{\mathrm{T}}\delta D'(\boldsymbol{q})\,\boldsymbol{e}_{\boldsymbol{q}j}'}{6\Omega_{\boldsymbol{q}j}^2}, \tag{6}$$

where $D'(\boldsymbol{q})$ and $\boldsymbol{e}_{\boldsymbol{q}j}'$ are the dynamical matrix and eigenvector, respectively, constructed from the effective second-order force constants at various temperatures.[28] $\delta D(\boldsymbol{q})$ is a change in the dynamical matrix due to a volume change δV (see the theoretical background in the supplement materials for more details). Finally, according to Grüneisen's law, the CTE incorporating higher-order anharmonicity is

$$\alpha_V^{\mathrm{SCPH}}(T) = \frac{\sum_{\boldsymbol{q}j} C_{V,\boldsymbol{q}j}^{\mathrm{SCPH}}\gamma_{\boldsymbol{q}j}^{\mathrm{SCPH}}}{B_V \times V}, \tag{7}$$

where B_V and V are the bulk modulus and volume, respectively. For the cubic crystal system, its bulk modulus is given by

$$B_V = \frac{C_{11}+2C_{12}}{3}, \tag{8}$$

where C_{ij} represents the component in the i-th row and the j-th column of the elasticity matrix.[30]

It is worth noting that our method differs from the QHA, as it is based on the SCPH theory. The phonon frequencies and Grüneisen parameters obtained are functions of temperature rather than volume. Therefore, this method does not support deriving B_V by constructing a free energy function and taking its derivatives. Instead, we have adopted the highly efficient elastic matrix approach.

3. Simulation details

The four structures involved in this study all belong to the cubic crystal system, with space groups as follows: $Fd\bar{3}m$ (No. 227) for Si, $Fm\bar{3}m$ (No. 225) for $CaZrF_6$ and NaBr, and $Pm\bar{3}m$ (No. 221) for $SrTiO_3$. *Ab initio* density functional theory (DFT) calculations were performed using the Vienna *Ab initio* Simulation Package (VASP),[31,32] which implements the projector augmented wave (PAW) method.[33,34] A cutoff energy of 520 eV was used, and the Brillouin zone was sampled using a Gamma k-point grid with a density of $2\pi \times 0.03$ Å^{-1}. We employed the PBE exchange–correlation function,[35] setting energy and force convergence criteria to $\Delta E = 10^{-8}$ eV and $\Delta F = 10^{-7}$ eV/Å, respectively. The self-consistent phonon equation was solved using the numerical algorithm from Ref. [28] within the ALAMODE package. The $\boldsymbol{q}$ mesh for SCPH matched the supercell size, and the inner q_1 mesh was increased up to $14 \times 14 \times 14$ to ensure convergence of anharmonic phonon frequencies. The self-consistent field loop was iterated until the total electronic energy change between successive steps was smaller than 10^{-10} eV and we consider the off-diagonal elements of the loop diagram in the SCPH calculation. As temperature increases, we employed mixing parameters ranging from 0.1 to 0.5. Furthermore, for heat capacity and Grüneisen parameter calculations, a $30 \times 30 \times 30$ q-point grid was employed to ensure convergence and accurate determination of the CTE. To assess the impact of high-order anharmonic terms on CTE, we employed the supercell finite displacement method and CSLD method to extract harmonic and anharmonic IFCs,[36,37] with detailed parameters provided in the supplement materials.

4. Result and discussion

4.1. Analysis of bonding composition

In Fig. 1, we present the crystal structures, electron localization functions (ELF) including bonding planes, and the extremums of ELF along the bonding directions for Si, $CaZrF_6$, $SrTiO_3$, and NaBr, respectively[38] (the one-dimensional ELF curve among chemical bonds is shown in Fig. S1 in the supplement materials). We find that the maximum ELF value between Si–Si bonds can reach 0.95, which is a typical characteristic of covalent bonds. Regarding $CaZrF_6$ and $SrTiO_3$, the ELF near each atom is large, with electrons concentrated around them. However, the minimum ELF values between Zr–F and Ti–O bonds are 0.2, indicating that they contain both ionic and covalent components. In the NaBr, electrons are mainly concentrated near Br, and the minimum ELF value approaches 0, which is typical of an ionic crystal. The middle of Fig. 1 presents the volumetric CTEs of these four structures at 300 K under the second-order QHA, the third-order PT, and the fourth-order SCPH theory. It can be seen that QHA and PT cannot accurately calculate the CTE for materials other than Si, while our calculation results are basically consistent with experimental values, demonstrating the significant contribution of higher-order anharmonicity to thermal expansion.

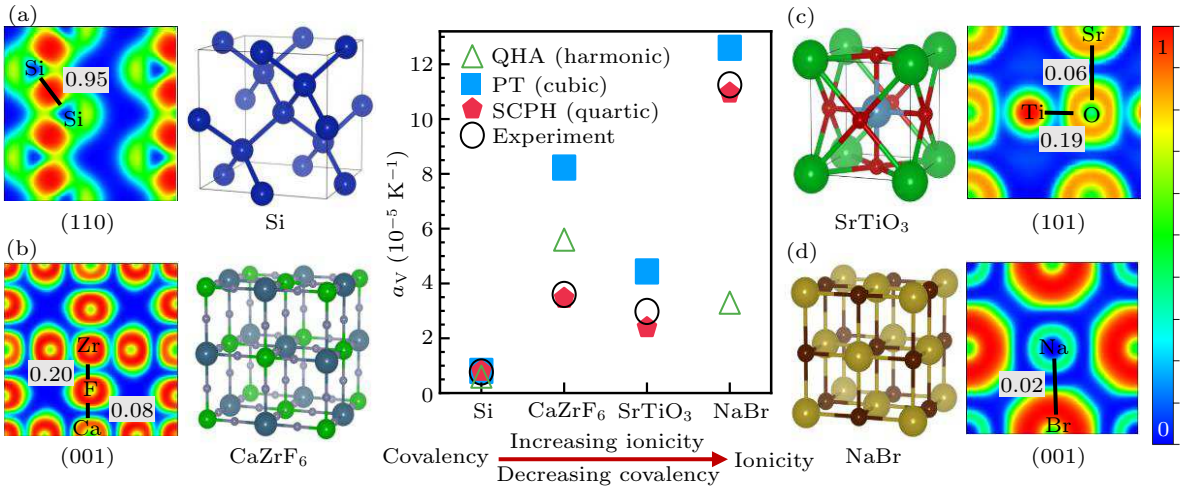


Fig. 1. (a) Si, (b) $CaZrF_6$, (c) $SrTiO_3$, and (d) NaBr: the unit cells of the four structures and their electron localization function (ELF) on planes containing bonding. The bonding directions and extremums of ELF are also annotated. In the middle, the volumetric expansion coefficients of these four structures at 300 K are calculated using the second-order QHA (green triangles), the third-order PT (blue squares), and the fourth-order SCPH theory (red pentagons). Experimental data are shown within black circles.[39–42] Note that the CTE for $CaZrF_6$ should be negative, but here its absolute value is taken.

To quantitatively describe the bonding types of several structures, as illustrated in Fig. 2, we have calculated the crystal orbital bond indices (COBI) and their integrals (ICOBI) for their chemical bonds. The ICOBI values range from 1 to 0, representing a decrease in covalency (and an increase in ionicity).[43] In Fig. 2(a), the COBI curve for Si–Si bonds exhibits large and continuous dispersion due to high sp orbital hybridization, with a bond index ICOBI = 0.92 indicating covalent bonding. In Figs. 2(b) and 2(c), the COBI for Ca–F and Sr–O bonds contains only one discrete interaction below the

Fermi energy, with their ICOBI values close to 0, reflecting strong ionicity due to electron transfer. The ICOBI values for Zr–F and T–O bonds are 0.57 and 0.53, respectively, indicating the simultaneous presence of ionic and covalent interactions. In Fig. 2(d), the COBI for Na–Br bonds is an isolated energy level with ICOBI = 0.09, proving that it is purely ionic bonding. Below, we will analyze the different effects of higher-order anharmonicity on the thermal expansion of these three types of materials in terms of covalent bonds, mixed bonds, and ionic bonds.

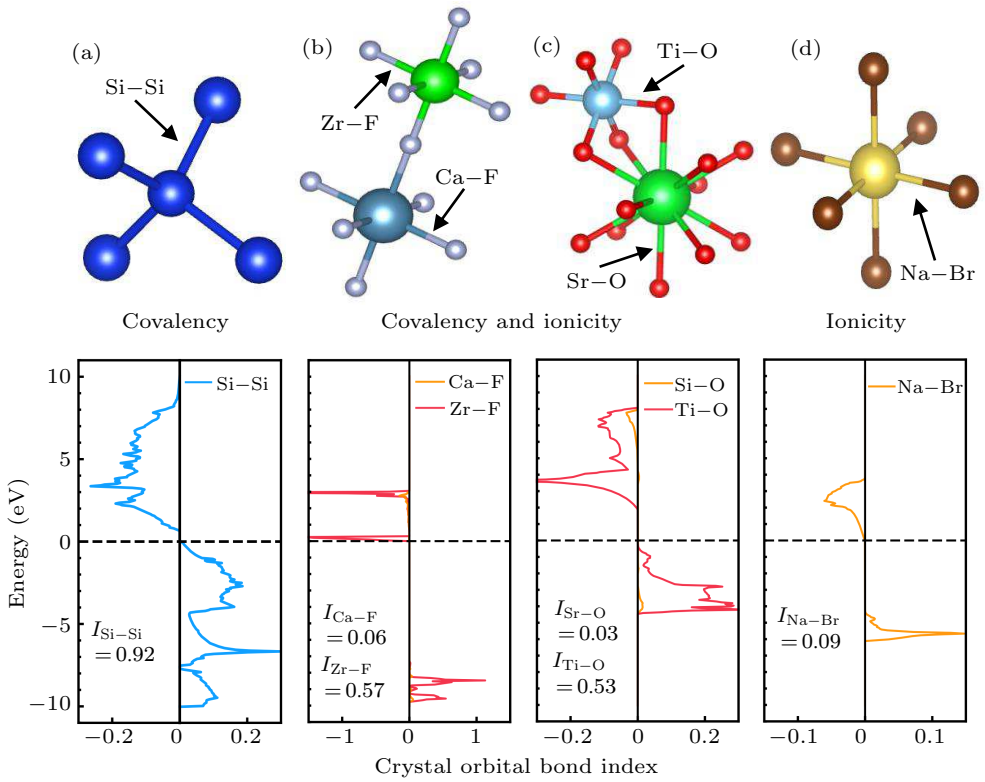


Fig. 2. (a) Si, (b) $CaZrF_6$, (c) $SrTiO_3$, (d) NaBr: The relationship between the COBI and energy for the chemical bonds in these four structures, along with their integrals ICOBI (denoted by the letter I). The blue, orange, and red curves represent covalent, ionic, and mixed bonds, respectively.

4.2. Impact of high-order anharmonicity on CTE

Figure 3(a) displays the SCPH frequencies and mode densities of the covalent crystal Si along high-symmetry paths in the Brillouin zone at temperatures ranging from 0 K to 800 K. The dispersion relations show no significant changes with increasing temperature, indicating that higher-order terms have a minor impact on the phonon energies of Si. Figure 3(b) shows the linear CTE of Si calculated using the second-order QHA,[44] the third-order PT, and the fourth-order SCPH theory, respectively. We found that all these results are in good agreement with experimental values,[39,45] suggesting that higher-order terms are not necessary to accurately predict the CTE of Si. The strong covalent interactions limit the weight of higher-order terms in the potential energy expansion, making Si a nearly "harmonic" system.

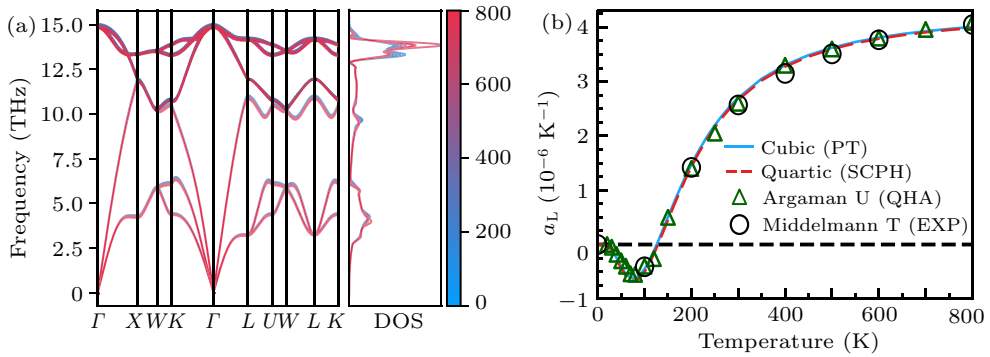


Fig. 3. Single-crystal Si at 0 K–800 K: (a) self-consistent phonon frequencies and mode densities, (b) linear thermal expansion coefficients calculated using the second-order QHA (green triangles), the third-order PT (blue solid lines), and the fourth-order SCPH theory (red dashed lines), with experimental data shown as black circles.[39,45]

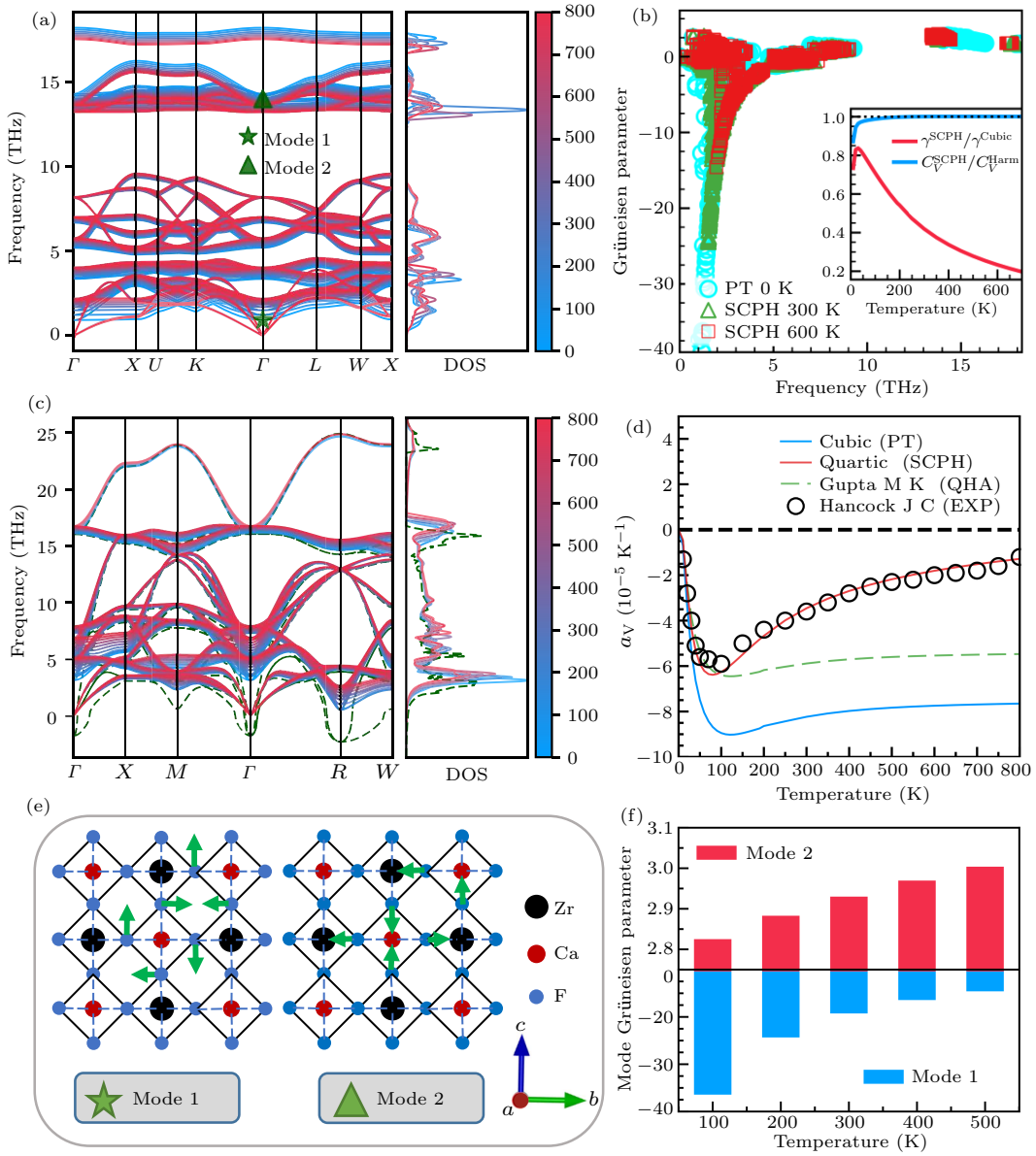


Fig. 4. Panels (a) and (c) show the self-consistent phonon frequencies and mode densities of $CaZrF_6$ and $SrTiO_3$, respectively, at temperatures ranging from 0 K to 800 K. The green dashed lines indicate the presence of imaginary frequencies under the harmonic approximation. (b) The outer graph depicts the mode Grüneisen parameters of $CaZrF_6$ calculated using PT (blue circles) and SCP theory at different temperatures (green triangles for 300 K and red rectangles for 600 K). The inner graph shows the ratios of total heat capacities $C_V^{SCPH}/C_V^{harmonic}$ (blue) and total Grüneisen parameters $\gamma^{SCPH}/\gamma^{cubic}$ (red). (d) The volumetric CTE of $CaZrF_6$ at temperatures from 0 K to 800 K are calculated using the QHA (green dashed line), PT (blue solid line), and SCPH (red solid line), with experimental data shown as black circles.[42] (e) The atomic vibrations corresponding to the hard mode (mode 1) and soft mode (mode 2) at the Γ point in $CaZrF_6$, (f) and the relationship between their mode Grüneisen parameters and temperatures.

$CaZrF_6$ belongs to the $A_{II}B_{IV}F_6$ material family, consisting of alternating Ca–F and Zr–F octahedra.[46] Its negative thermal expansion behavior offers numerous possibilities for designing materials with controlled thermal expansion. Similar to ScF_3, it retains its cubic phase below 10 K. This contrasts with cubic $CoZrF_6$, which only shows moderate negative thermal expansion above its rhombohedral-to-cubic phase transition at approximately 270 K. The CTE calculated by Hancock *et al.* using the QHA method deviates significantly from experimental values,[47] prompting us to include the contributions of higher-order terms in our calculations. The dispersion relations at temperatures from 0 K to 800 K are shown in Fig. 4(a), revealing that as temperature increases, the high-frequency optical branches soften while the low-frequency optical branches harden, leading to a redistribution of phonon energies and mode densities within the Brillouin zone. Equation (7) shows that the modal heat capacity and modal Grüneisen parameter are the decisive factors for CTE. To facilitate comparative analysis of the impact of higher-order anharmonic terms on them, the total heat capacity and total Grüneisen parameter defined below are used here:

$$C_V(T) = \frac{k_B}{N_q}\sum_{qj}\left(\frac{x}{\mathrm{sh}x}\right)^2; \quad x = \frac{\hbar\omega_{qj}}{2k_BT}, \tag{9}$$

$$\gamma(T) = \frac{\sum_{qj} C_{V,qj}\gamma_{qj}}{C_V(T)}. \tag{10}$$

The magnitude of the higher-order anharmonic effects is quantified by examining the deviations of $C_V^{\mathrm{SCPH}}/C_V^{\mathrm{harmonic}}$ and $\gamma^{\mathrm{SCPH}}/\gamma^{\mathrm{cubic}}$ from 1, figure 4(b) shows their relationship with temperature and compares the modal Grüneisen parameters under the PT and SCPH theories. Despite significant fluctuations in phonon energy with temperature, the mutual constraint between phonon number and energy across modes, combined with averaging over mesh points for total heat capacity, keeps $C_V^{\mathrm{SCPH}}/C_V^{\mathrm{harmonic}}$ close to 1. The introduction of higher-order terms appropriately corrects the negative mode Grüneisen parameters in the low-frequency region, causing them to converge continuously as the temperature increases, which is overlooked in the third-order PT method. The γ^{SCPH} value is slightly lower than γ^{cubic} in the low-temperatures (around 4/5) and gradually decreases to 1/5 as the temperature rises. This makes it a crucial parameter for accurately calculating the CTE when considering higher-order terms. As shown in Fig. 4(d), the CTE obtained from including higher-order terms introduces the correct temperature dependence, correcting the deviations in the QHA and PT methods and achieving good agreement with experimental values.[42,48] Furthermore, we conducted a visual analysis of the atomic vibrations of the hard mode (mode 1) and soft mode (mode 2) at the Γ point. As shown in Fig. 4(e), we found that the vibrations at the hardening site correspond to the transverse vibrations of the bridging atoms in the rigid unit model, which is an important source of negative expansion. Therefore, mode 1 should have a negative Grüneisen parameter and continuously decrease with hardening (see Eq. (6)). On the other hand, the vibrations at the softening site increase the octahedral interstitial space, contributing to positive expansion, so mode 2 should have a positive Grüneisen parameter and continuously increase with softening. We extracted the modal Grüneisen parameters of these two modes at different temperatures (Fig. 4(f)), and their changes are consistent with the above analysis, verifying the physical correctness of our method.

$SrTiO_3$, a widely studied perovskite oxide, undergoes a soft-mode phase transition from cubic to tetragonal structure as the temperature decreases to 105 K. In this study, we investigate the thermal expansion behavior of its high-temperature cubic phase. Due to its strong lattice anharmonicity, there are imaginary frequencies in the phonon dispersion calculated under the harmonic approximation. Mu *et al.* used the TDEP method combined with the third-order PT to calculate a CTE of 1.71×10^{-5} K^{-1} at 300 K and attributed the deviation from the experimental result of 2.2×10^{-5} K^{-1} to the neglect of higher-order terms.[20,40] Therefore, in this study, we analyzed the contribution of the fourth-order terms. Figure 4(b) shows the phonon dispersion and mode density of $SrTiO_3$ from 0 K–800 K, where it can be seen that unstable phonon modes are eliminated after SCPH correction, and the optical branches undergo significant hardening as the temperature increases. The changes in lattice heat capacity and Grüneisen parameter after considering higher-order terms follow the same pattern as in $CaZrF_6$, which is shown in Fig. S2 in the supplement materials. The calculated results of the CTEs are shown in Fig. 5. It can be observed that our results accurately describe the variation in the thermal expansion coefficient of $SrTiO_3$ from 2.2×10^{-5} K^{-1} at room temperature to 3.23×10^{-5} K^{-1} at high temperatures, as observed in experiments. Our research indicates that in negative expansion materials $CaZrF_6$ and perovskite $SrTiO_3$, which contain both ionic and covalent bonding, the contribution of higher-order anharmonic terms to thermal expansion cannot be overlooked. These terms must be taken into account to accurately calculate the CTE of these materials.

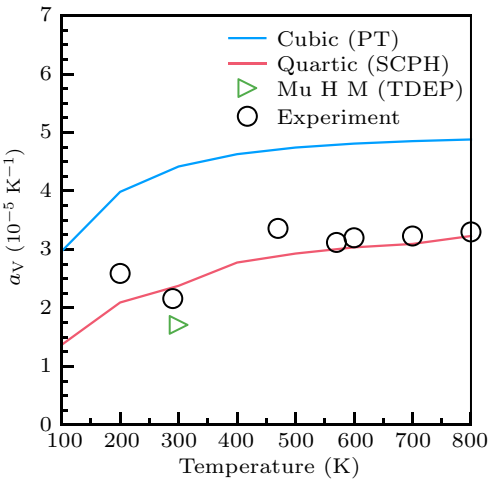


Fig. 5. The volumetric CTE of $SrTiO_3$ at temperatures from 100 K to 800 K are calculated using the PT (blue solid line), SCPH (red solid line), and TDEP method (green triangles), with experimental data shown as black circles.

NaBr is an ionic crystal with a rock-salt structure. Its phonon dispersion, as shown in Fig. 6(a), exhibits a significant hardening of the optical modes with increasing temperature, which aligns well with Shen's proposal that anharmonicity strongly influences the phonon self-energy of the LO mode.[12] As illustrated in Fig. 6(b), after considering fourth-order anharmonicity, the CTE of NaBr agrees well with experimental results in the low-temperature range (below 200 K).[41,49] However, our method fails to provide the correct trend when the temperature exceeds 200 K. Researchers have demonstrated that volume-dependent anharmonicity leads to giant thermal expansion in NaBr. Therefore, we obtained the equilibrium volume through AIMD simulations under the NPT ensemble and recalculated the CTE at 500 K and 700 K with volume corrections taken into account. The comparison of various physical quantities before and after the correction is shown in Fig. 6(c) (For specific numerical values, please refer to Tables S1 and S2 in the supplement materials). We found that the softening of the lattice caused by temperature increase

is the main source of the discrepancy (B_V decreased dramatically), while the Grüneisen parameter only increases slightly. This results in a CTE after correction that still differs from the experimental value. It indicates that in the high-temperature range of ionic crystals, the Grüneisen parameter obtained approximately from Eq. (6) can no longer serve as an indicator of anharmonicity. It is necessary to develop theories that directly apply higher-order IFCs in the calculation of γ_{qj} to further enhance the coupling strength between theory and experiment.

Furthermore, it is important to note that the temperature dependence of the bulk modulus must also be carefully considered. Although the QHA theory provides a method for calculating B_V, the temperature-dependent bulk modulus may lead to excessive softening and is potentially prone to divergence, particularly in the low-temperature regime. This partly is attributed to some modes may not be elegantly grouped in realistic computation. Calculating self-consistent phonon frequencies at different volumes and fitting the free energy function that includes higher-order contributions is a promising direction. However, whether the QHA model remains valid under these conditions, along with the high computational cost of extracting higher-order force constants, presents significant challenges. We look forward to further exploring this direction in future research to provide a more accurate theoretical description and prediction of the thermal expansion behavior of materials.

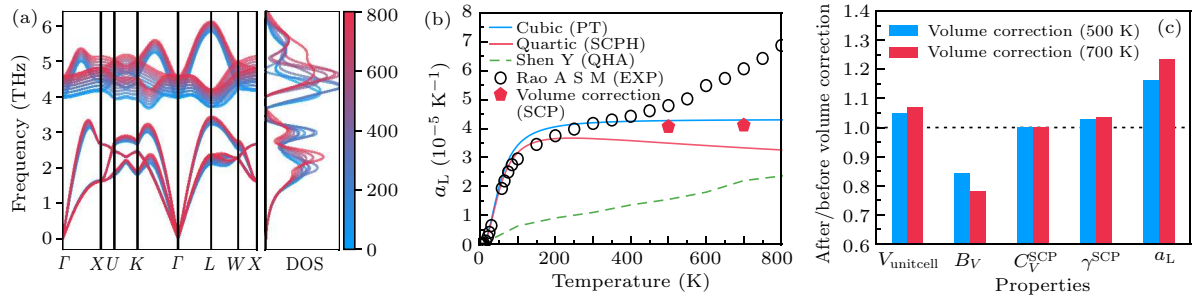


Fig. 6. Ionic crystal NaBr at 0 K–800 K: (a) SCPH frequencies and mode densities, (b) linear thermal expansion coefficients calculated using the second-order QHA (green dashed line), the third-order PT (blue solid line), and the fourth-order SCPH theory (red solid line). The red pentagon represents the calculation result considering volume correction at 500 K and 700 K, while the black circles represent experimental values,[41] (c) ratios of relevant physical properties of NaBr before and after volume correction at 500 K and 700 K (from left to right: unit cell volume, bulk modulus, lattice heat capacity, Grüneisen parameter, and coefficient of linear expansion).

5. Conclusion

In summary, we propose a scheme for calculating thermal expansion coefficients based on SCPH theory that includes fourth-order anharmonicity. Leveraging the efficiency of the compressive sensing lattice dynamics method for extracting force constants, the fourth-order renormalized phonon frequencies at different temperatures can be easily obtained. By combining PT with the solution to the SCPH equation, we redefine the decisive factors for thermal expansion, namely lattice heat capacity, and Grüneisen parameter, and use Grüneisen's law to calculate the CTE of materials. From the perspective of crystal bonding types, we find that for the covalent crystal Si, both the second-order QHA and the third-order PT as well as the fourth-order SCPH method can yield accurate results. The strong covalent interaction limits the weight of higher-order terms in the potential energy series, making Si exhibit nearly "harmonic" characteristics. For the mixed-bonded negative thermal expansion material $CaZrF_6$ and the perovskite $SrTiO_3$, higher-order anharmonic terms have a minor impact on lattice heat capacity, while the Grüneisen parameter undergoes dramatic changes with increasing temperature, making it the decisive parameter for considering higher-order terms in calculating the CTE. Compared to the results of the QHA and PT, our results closely align with experimental data, demonstrating the necessity of considering higher-order terms in mixed-bonded structures. For the ionic crystal NaBr, we obtained good results below 200 K. However, in the high-temperature range, γ obtained under PT cannot accurately reflect volume-depandent anharmonicity and cannot serve as an indicator of anharmonic effects. More sophisticated theories are required to explore the origin of the giant thermal expansion in such rocksalt structures, such as directly calculating γ through higher-order IFCs. Our study elucidates the significant contributions of higher-order anharmonicity to different bonding structures, paving the way for deeper investigations into the thermal expansion of materials.

Acknowledgements

Project supported by the National Natural Science Foundation of China (Grant No. 62125402). Calculations were performed in part at the high performance computing center of Jilin University.

References

[1] Greve B K, Martin K L, Lee P L, Chupas P J, Chapman K W and Wilkinson A P 2010 *J. Am. Chem. Soc.* **132** 15496
[2] Chatterji T, Zbiri M and Hansen T C 2011 *Appl. Phys. Lett.* **98** 181911
[3] Dove M T and Fang H 2016 *Rep. Prog. Phys.* **79** 066503
[4] Ritz E T and Benedek N A 2018 *Phys. Rev. Lett.* **121** 255901
[5] Lu T, Liu S L, Sun Y H, Wang W H and Pan M X 2022 *Chin. Phys. Lett.* **39** 036401

[6] He J C, Pan Z, Su D, Shen X D, Zhang J, Lu D B, Zhao H T, Cong J Z, Liu E K, Long Y W and Sun Y 2023 *Chin. Phys. Lett.* **40** 066501
[7] Hao Y, Xie H, Zeng G, Yuan H, Hu Y, Guo J, Gao Q, Chao M, Ren X and Liang E J 2022 *Chin. Phys. B* **31** 046502
[8] Allen P B 2015 *Phys. Rev. B* **92** 064106
[9] Ritz E T, Li S J and Benedek N A 2019 *J. Appl. Phys.* **126** 171102
[10] Aierken Y, Çakır D, Sevik C and Peeters F M 2015 *Phys. Rev. B* **92** 081408
[11] Zhang Y, Mu H, Cai Y, Wang X, Zhou K, Tian F, Fu Y and Zhang L 2023 *Chin. Phys. B* **32** 056302
[12] Shen Y, Saunders C N, Bernal C M, Abernathy D L, Manley M E and Fultz B 2020 *Phys. Rev. Lett.* **125** 085504
[13] Tadano T, Gohda Y and Tsuneyuki S 2015 *Phys. Rev. Lett.* **114** 095501
[14] Debernardi A, Baroni S and Molinari E 1995 *Phys. Rev. Lett.* **75** 1819
[15] Li W and Mingo N 2014 *Phys. Rev. B* **90** 094302
[16] Narasimhan S and Vanderbilt D 1991 *Phys. Rev. B* **43** 4541
[17] Esfarjani K and Stokes H T 2008 *Phys. Rev. B* **77** 144112
[18] Hellman O, Steneteg P, Abrikosov I A and Simak S I 2013 *Phys. Rev. B* **87** 104111
[19] Hellman O and Abrikosov I A 2013 *Phys. Rev. B* **88** 144301
[20] Mu H, Zhang Y, Zou H, Tian F, Fu Y and Zhang L 2023 *J. Phys. Chem. Lett.* **14** 190
[21] Masuki R, Nomoto T, Arita R and Tadano T 2022 *Phys. Rev. B* **105** 064112
[22] Oba Y, Tadano T, Akashi R and Tsuneyuki S 2019 *Phys. Rev. Mater.* **3** 033601
[23] Hooton D J 1958 *Philosophical Magazine* **3** 49
[24] Werthamer N R 1970 *Phys. Rev. B* **1** 572
[25] Zhou F, Nielson W, Xia Y and Ozoliņš V 2019 *Phys. Rev. B* **100** 184308
[26] Zhou F, Sadigh B, Åberg D, Xia Y and Ozoliņš V 2019 *Phys. Rev. B* **100** 184309
[27] Zhao Y, Lian C, Zeng S, Dai Z, Meng S and Ni J 2020 *Phys. Rev. B* **101** 184303
[28] Tadano T and Tsuneyuki S 2015 *Phys. Rev. B* **92** 054301
[29] Grüneisen E 1912 *Annalen der Physik* **344** 257
[30] Wu Z, Zhao E, Xiang H, Hao X, Liu X and Meng J 2007 *Phys. Rev. B* **76** 054115
[31] Kresse G and Furthmüller J 1996 *Comput. Mater. Sci.* **6** 15
[32] Kresse G and Furthmüller J 1996 *Phys. Rev. B* **54** 11169
[33] Blöchl P E 1994 *Phys. Rev. B* **50** 17953
[34] Kresse G and Joubert D 1999 *Phys. Rev. B* **59** 1758
[35] Perdew J P, Burke K and Ernzerhof M 1996 *Phys. Rev. Lett.* **77** 3865
[36] Sun T, Zhang D B and Wentzcovitch R M 2014 *Phys. Rev. B* **89** 094109
[37] Zhou F, Nielson W, Xia Y and Ozoliņš V 2014 *Phys. Rev. Lett.* **113** 185501
[38] Becke A D and Edgecombe K E 1990 *J. Chem. Phys.* **92** 5397
[39] Okada Y and Tokumaru Y 1984 *J. Appl. Phys.* **56** 314
[40] De Ligny D and Richet P 1996 *Phys. Rev. B* **53** 3013
[41] Rapp J E and Merchant H D 1973 *J. Appl. Phys.* **44** 3919
[42] Hancock J C, Chapman K W, Halder G J, Morelock C R, Kaplan B S, Gallington L C, Bongiorno A, Han C, Zhou S and Wilkinson A P 2015 *Chem. Mater.* **27** 3912
[43] Müller P C, Ertural C, Hempelmann J and Dronskowski R 2021 *J. Phys. Chem. C* **125** 7959
[44] Argaman U, Eidelstein E, Levy O and Makov G 2016 *Phys. Rev. B* **94** 174305
[45] Middelmann T, Walkov A, Bartl G and Schödel R 2015 *Phys. Rev. B* **92** 174113
[46] Giddy A P, Dove M T, Pawley G S and Heine V 1993 *Acta Crystallogr A Found Crystallogr* **49** 697
[47] Gupta M K, Singh B, Mittal R and Chaplot S L 2018 *Phys. Rev. B* **98** 014301
[48] Hu L, Chen J, Xu J, Wang N, Han F, Ren Y, Pan Z, Rong Y, Huang R, Deng J, Li L and Xing X 2016 *J. Am. Chem. Soc.* **138** 14530
[49] Rao A S M, Narender K, Rao K G K and Krishna N G 2013 *JMP* **04** 208